Applied Physics Letters

Mobility of near surface MOVPE grown InGaAs/InP quantum wells

Cite as: Appl. Phys. Lett. **117**, 013102 (2020); https://doi.org/10.1063/5.0006530
Submitted: 03 March 2020 • Accepted: 13 June 2020 • Published Online: 06 July 2020

Lasse Södergren, Navya Sri Garigapati, Mattias Borg, et al.

ARTICLES YOU MAY BE INTERESTED IN

Room-temperature operation of c-plane GaN vertical cavity surface emitting laser on conductive nanoporous distributed Bragg reflector
Applied Physics Letters **117**, 011101 (2020); https://doi.org/10.1063/5.0012281

Band parameters for III–V compound semiconductors and their alloys
Journal of Applied Physics **89**, 5815 (2001); https://doi.org/10.1063/1.1368156

Homo-epitaxial growth of n-GaN layers free from carbon-induced mobility collapse and off-angle-dependent doping variation by quartz-free hydride vapor phase epitaxy
Applied Physics Letters **117**, 012103 (2020); https://doi.org/10.1063/5.0014528

© 2020 Author(s).

Mobility of near surface MOVPE grown InGaAs/InP quantum wells

Cite as: Appl. Phys. Lett. **117**, 013102 (2020); doi: 10.1063/5.0006530
Submitted: 3 March 2020 · Accepted: 13 June 2020 ·
Published Online: 6 July 2020

Lasse Södergren,[1,2,a)] Navya Sri Garigapati,[1,2] Mattias Borg,[1,2] and Erik Lind[1,2]

AFFILIATIONS

[1]Department of Electrical and Information Technology, Lund University, Box 118, SE-221 00 Lund, Sweden
[2]NanoLund, Lund University, Box 118, SE-221 00 Lund, Sweden

[a)]Author to whom correspondence should be addressed: lasse.sodergren@eit.lth.se

ABSTRACT

In this work, we study the electron mobility of near surface metal organic vapor phase epitaxy-grown InGaAs quantum wells. We utilize Hall mobility measurements in conjunction with simulations to quantify the surface charge defect density. Buried quantum wells are limited by polar optical phonon scattering at room temperature. In contrast, the quantum wells directly at the surface are limited by remote charge impurity scattering from defects situated at the III–V/oxide interface or inside the oxide, showing a mobility of 1500 cm^2/V s. Passivating the InGaAs surface by depositing an oxide reduces the amount of defects at the interface, increasing the mobility to 2600 cm^2/V s.

© 2020 Author(s). All article content, except where otherwise noted, is licensed under a Creative Commons Attribution (CC BY) license (http://creativecommons.org/licenses/by/4.0/). https://doi.org/10.1063/5.0006530

Near surface quantum well-based devices are of interest for high-frequency III–V field effect transistors and quantum devices utilizing superconducting/semiconducting effects. III–V metal-oxide-semiconductor field effect transistors (MOSFETs) have demonstrated the highest transconductance for any transistors, with $g_m = 3.45$ mS/μm.[1] MOSFETs used for radio frequency applications have a spacer region to reduce parasitic gate–source and gate–drain capacitances, allowing for high frequency operation.[2] This increases the access series resistance, degrading the on-current and gain. In order to minimize the resistance, a spacer region with a high carrier concentration and high electron mobility is necessary. This can be achieved by introducing modulation doping in the access region, which spatially separates the free carriers from the dopants, allowing for a high carrier concentration without severely affecting the electron mobility. The spacer is in essence an ungated quantum well situated close to or directly at the surface. A similar structure can also be found in quantum devices such as gatemons,[3] which are based on induced superconductivity in the semiconductor due to a superconductor in close proximity. Semiconductor/superconductor coupling is highly sensitive to the electron wave function overlap at the semiconductor surface, which requires a near surface quantum well. Near surface InAs quantum wells grown by molecular beam epitaxy (MBE) have been demonstrated to have high electron mobilities.[4–7] The electrical properties of these types of structures are sensitive to surface conditions, with a mobility limited by surface scattering. Metal organic vapor phase epitaxy (MOVPE) has the capability to produce high-quality InGaAs demonstrating mobilities over 10^4 cm^2/V s.[8] Deeply buried quantum wells in the InGaAs/InP material system have also been demonstrated with excellent mobility, with $\mu = 520\,000$ cm^2/V s at T = 300 mK.[9]

In this work, we investigate the mobility of near surface InGaAs/InP quantum wells grown by MOVPE. The results from Hall mobility measurements and modeling show that charged defects at the semiconductor surface are the main limiting scatterer of the quantum well and that the effect can be reduced by utilization of a passivation through an atomic layer deposition (ALD) oxide. From mobility modeling, we estimate the concentration of charged surface defects, which is in line with earlier C–V experiments.[10] A schematic layout of the samples used is shown in Fig. 1. To study the effect of the quality of the III–V surface on the transport properties of the quantum well, four different device variants have been fabricated. All samples were grown by MOVPE on Fe-doped semi-insulating InP (100) substrates at 100 mbar and 600 °C. The sources used were TMGa, TMIn, AsH_3, PH_3, and 0.1% Si_2H_6 diluted in H_2. The structures consist of 25 nm of unintentionally doped InP, followed by a 13 nm $In_{0.63}Ga_{0.37}As$ channel, as determined from XRD measurements. InGaAs was grown with an indium content of 63% in order to take advantage of the lower effective mass, decreased alloy scattering, and increased spin–orbit coupling relative to the lattice matched composition. This results in a compressively strained layer with an estimated critical thickness of 20 nm.[11] The InP top barrier thicknesses covering the InGaAs channel

© Author(s) 2020

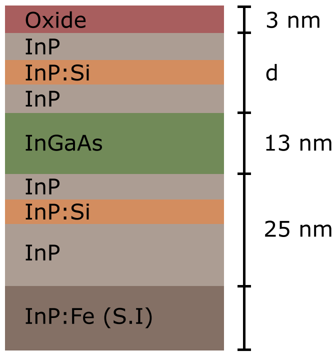

FIG. 1. General schematic of the near-surface InGaAs/InP quantum well structure.

were 0, 12, and 25 nm. A 4 nm-thick Si-doped layer with a sheet carrier concentration of 2×10^{12} cm^{-2} was placed 4 nm from the InGaAs channel on both sides. Samples C and D do not have the top InP barrier, thus placing the quantum well directly at the surface with only a bottom modulation doped layer. To study the effect of high-k passivation, sample C has been passivated by a high-k oxide layer. Following the growth of the III–V layers, Ti/Pd/Au contacts were evaporated in a Van der Pauw configuration. The surface was then passivated by ozone cleaning and 10% $(NH4)_2S$ solution before ALD deposition of Al_2O_3/HfO_2 at 300/120 °C. The surface passivation and oxide deposition were omitted on sample D. The measured mobilities at 10 K and 300 K are presented in Table I.

Figure 2 shows effective mass Schrödinger–Poisson models of the band edges and the carrier distributions of the grown structures. For the InP surfaces (samples A and B), a Fermi level pinning at the InP surface of 0.2 eV below the conduction band edge has been used. For samples C and D, the Fermi level at the surface has been adjusted to be above the conduction band edge by 0.17 eV and 0.23 eV, respectively, and so the quantum well sheet density matches the $T = 300$ K experimental sheet density.

Electric characterization of the structures was performed using Hall measurements by the Van der Pauw method. Magnetic fields up to 1 T were used, and the sample temperature was controlled using a closed cycle helium refrigerator in the range of 10–300 K. The measured electron density and sheet resistivity are shown in Fig. 3 and the corresponding Hall mobility in Fig. 4. The electron density remains almost constant with temperature, increasing slightly with higher temperature. We also observe that the electron density of the surface quantum wells of samples C and D has a relatively large temperature dependence in the range of 100 K–300 K as compared to the buried quantum wells, indicating a stronger effect of thermal activation of surface defects. The measured electron sheet density of sample B at room temperature is 3.8×10^{12} cm^{-2}, while the calculation predicts a sheet concentration of 2.3×10^{12} cm^{-2}; this difference is attributed to run-to-run variability in the dopant concentration. The surface quantum wells have a room temperature sheet resistance of ~1 kΩ/sq. The buried quantum wells have an improved sheet resistance by a roughly factor of ~5 down to ~200 Ω/sq, showing the favorable effect of moving the charge defect dense surface away from the transport channel. This is advantageous for constructing low access resistance spacer regions in a MOSFET device.

In order to analyze contributions from different scattering mechanisms, mobility calculations have been performed. Four major scattering mechanisms have been taken into account: acoustic deformation potential, polar optical phonons, alloy disorder, and ionized impurities. The ionized impurities have been divided into two parts: remote-ionized impurities from the delta-doping layers and charge interface defects situated at the semiconductor surface. Surface roughness scattering has been neglected due to its weak contribution to the total mobility in thicker quantum wells.[12] Atomic force microscopy (AFM) imaging has confirmed step-flow growth mode, and the surface has a roughness (RMS) value lower than 0.2 nm. Only scattering within the first subband has been considered. Material parameters from the literature have been used, shown in Table II, with the charged interface defect density at the InGaAs and InP top surfaces as the only free parameter.

Phonon scattering is typically the limiting scattering process at high temperatures. With bulk phonons and only the first subband considered, the polar optical phonon scattering rate can be written for absorption as[13,14]

$$\frac{1}{\tau^A_{pop}} = \frac{e^2\omega_0 N_0 m^* a}{8\pi^2\hbar^2\varepsilon_0\varepsilon_p} \times \frac{1 - f_0(E_F + \hbar\omega_0)}{1 - f_0(E_F)} \tag{1}$$

and for emission as

$$\frac{1}{\tau^E_{pop}} = \frac{e^2\omega_0 (N_0 + 1) m^*}{a\hbar^2 k_F^2 \varepsilon_0\varepsilon_p} \times \frac{1 - f_0(E_F - \hbar\omega_0)}{1 - f_0(E_F)}, \tag{2}$$

for scattering at the Fermi energy. The last factor on the right-hand side takes into account the occupation of the final and initial scattering states according to the Pauli principle, and f_0 is the Fermi–Dirac distribution. $N_0 = 1/(\exp\left(\frac{\hbar\omega_0}{k_B T}\right) - 1)$ is the phonon occupation number, m^* is the electron effective mass, ω_0 is the optical phonon frequency, e is the elementary charge, a is the thickness of the quantum well, and $\varepsilon_p = 1/\left(\frac{1}{\varepsilon_\infty} - \frac{1}{\varepsilon_s}\right)$, where ε_∞ and ε_s are the high frequency and static dielectric constant, respectively. The deformation potential acoustic phonon relaxation rate is given by[15]

TABLE I. Summary of sample characteristics, measured mobility, and carrier concentration data.

Sample	d (nm)	Oxide	μ @ 10 K (cm^2/V s)	μ @ 300 K (cm^2/V s)	n @ 300 K (cm^{-2})
A	25	Yes	27 800	10 000	2.6×10^{12}
B	12	Yes	16 500	7900	3.8×10^{12}
C	0	Yes	4000	2600	2.3×10^{12}
D	0	No	1800	1500	3.1×10^{12}

© Author(s) 2020

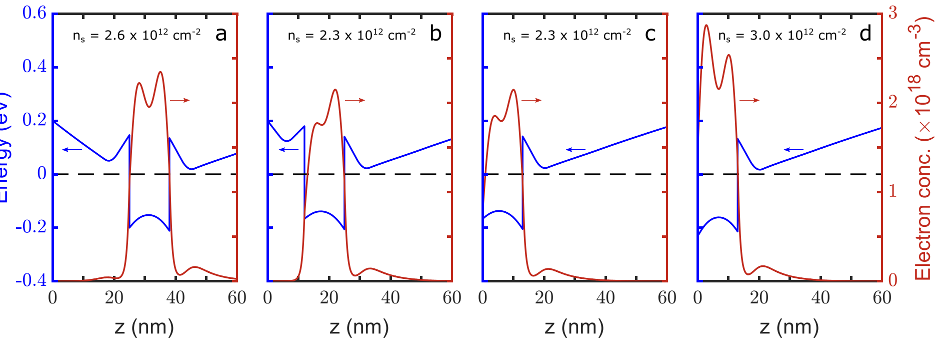

FIG. 2. Self-consistent Schrödinger–Poisson calculations for (a) sample A with a 25 nm top barrier, (b) sample B with a 12 nm top InP barrier, and (c) and (d) samples C and D without a top barrier.

$$\frac{1}{\tau_{adp}} = \frac{3m^* D_A^2 k_B T}{2\hbar^3 \rho v_s^2 a}, \tag{3}$$

where D_A is the deformation potential amplitude, ρ is the mass density, and v_s is the sound velocity. It has been shown that piezoelectric phonon scattering is relatively weak in both GaAs and InAs,[16] and therefore, it is neglected in this work. Within the Howard–Stern formulation[17] for elastic scattering, the relaxation time of electrons in a quantum well can be written as

$$\frac{1}{\tau} = \frac{m^*}{2\pi\hbar^3 k_F^3}\int_0^{2k_F} \frac{|U(q)|^2}{\varepsilon(q)} \frac{q^2}{\sqrt{1-\left(\frac{q}{2k_F}\right)^2}} dq, \tag{4}$$

where $U(q)$ is the potential describing the scattering mechanism as a function of wave vector q, $k_F = \sqrt{2\pi n_s}$ is the Fermi wave vector, with n_s being the sheet electron density, and finally, $\varepsilon(q)$ is the dielectric function of the two-dimensional electron gas in the quantum well. Following Gold,[17] we use

$$\varepsilon(q) = 1 + V(q)\left[1 - G(q)\right]X^0(q). \tag{5}$$

X^0 is the polarizability of the 2DEG given as 2D DOS and $G(q)$ is the Hubbard form of the local field correction.[18] $V(q)$ is the electron–electron interaction potential and is given by

$$V(q) = \frac{e^2}{2\varepsilon_0\varepsilon_s q} F_C(q), \tag{6}$$

with the form factor

$$F_C(q) = \int |\Psi(z)|^2 dz \int |\Psi(z')|^2 e^{-q|z-z'|} dz. \tag{7}$$

The electrons are assumed to be free to move in the xy-plane and confined in the z-direction with the wave function,

$$\Psi(z) = \sqrt{\frac{2}{a}}\sin\left(\frac{\pi z}{a}\right), \quad 0 \le z \le a, \tag{8}$$

and otherwise zero. For remote impurity scattering, the potential for wave vector q is given by

$$|U_R(q)|^2 = n_i\left(\frac{e^2}{2\varepsilon_0\varepsilon_s}\frac{1}{q}\right)^2 F_R(q, z_i)^2, \tag{9}$$

where n_i is the impurity sheet density concentration situated at a distance a_i away from the quantum well. The form factor

$$F_R(q, z_i) = \int |\Psi(z)|^2 e^{-q|z-z_i|} dz, \tag{10}$$

accounts for the distance between the impurity and the quantum well and the confinement. Scattering due to background doping of the quantum well is described by the potential

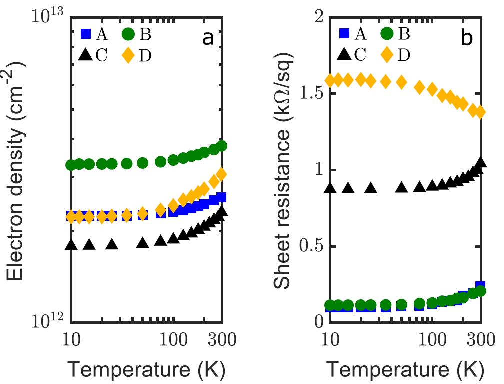

FIG. 3. (a) Measured sheet electron density and (b) sheet resistance as a function of temperature.

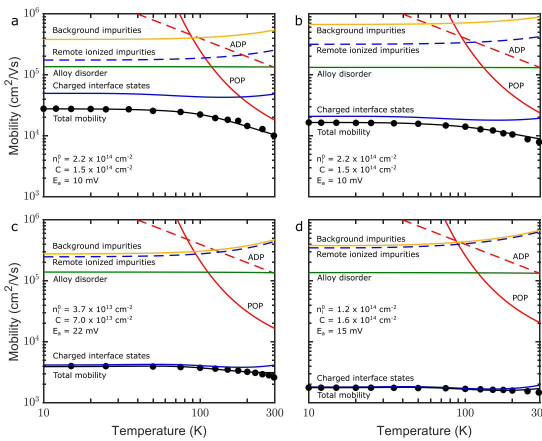

FIG. 4. Calculated electron mobility together with measured Hall mobility (circles) for (a) 25 nm InP top barrier (sample A), (b) 12 nm InP top barrier (sample B), (c) no InP top barrier (sample C), and (d) no InP top barrier and no passivation oxide (sample D).

© Author(s) 2020

TABLE II. Parameter values used in calculations.

Effective mass	m^*	$0.039m_0$
Optical phonon energy	ω_0	34.0 meV
Static dielectric constant	ε_s	14.1
High-frequency dielectric constant	ε_∞	11.8
Acoustic deformation potential	D_A	9.4 eV
Mass density	ρ	5.54 g/cm^3
Sound velocity	v_s	4160 m/s
Alloy disorder potential	V_a	0.5 eV
Lattice constant	a_L	5.908 Å

$$|U_B(q)|^2 = N_b a\left(\frac{e^2}{2\varepsilon_0\varepsilon_s}\frac{1}{q}\right)^2 F_B(q)^2, \tag{11}$$

where N_B is the background doping density and

$$F_B(q) = \frac{1}{a}\int F_R(q, z_i)dz_i. \tag{12}$$

The intermixing of group-III elements inside the quantum well gives rise to alloy scattering, described by an average potential[19]

$$|U_A|^2 = \frac{3x(1-x)V_a^2\Omega}{2a}, \tag{13}$$

for a perfectly random alloy. V_a is the average of the fluctuating alloy potential, x is the composition of group III elements, and $\Omega = \sqrt{3}\pi a_L^3/16$, with a_L being the lattice constant. Using Eq. (4) with (9), (11), or (13), the momentum relaxation time for the respective scattering mechanism can be found. The parameters used in calculations are presented in Table II. The relaxation time is related to the mobility by $\mu = e\langle\tau\rangle/m^*$, in which $\langle\tau\rangle$ is the thermal average of the relaxation time.[14] The electron density used in the calculations is obtained from measured data (see Fig. 3). The background doping concentration is set to $\sim 1\times10^{17}\,\text{cm}^{-3}$, and the modulation doping sheet density is $\sim 2\times10^{12}\,\text{cm}^{-2}$ as obtained from earlier measurements. The total mobility is estimated by adding the reciprocal mobility for each scattering process according to Matthiessen's rule. The calculated mobility components of the different scattering mechanisms and the total mobility are presented in Fig. 4 together with measured Hall mobility data.

It is clear from these results that the mobility at low temperatures is limited by scattering from remote ionized impurities situated at the high-k/III–V interface or inside the high-k oxide. At room temperature, the mobility of the buried quantum wells is limited by polar optical phonon scattering, while the total mobility of the surface quantum wells of samples C and D only shows a small dependence on the phonon density. Specifically, sample D, without any passivation oxide, is strongly limited by the surface defects ($n_i^0 = 1.2\times10^{14}\,\text{cm}^{-3}$), showing a low room temperature mobility of 1500 cm^2/V s. By introduction of a high-k oxide, the concentration of surface charges is reduced to $n_i^0 = 3.7\times10^{13}\,\text{cm}^{-2}$, which is similar to what has been reported from C–V data.[10] This is in line with a reduced amount of oxide defects from the ALD process. We also observe that the passivation increases the room temperature mobility to 2600 cm^2/V s. While a thick InP top barrier is beneficial for increased mobility, calculations show that increasing the thickness to more than ~50 nm has a small effect on the effective mobility due to alloy scattering becoming the dominating scattering mechanism. The minor increase in the calculated mobility components originating from background impurities, remote ionized impurities, and charge interface states at higher temperatures is due to increased screening effects with increased electron density. However, experimentally, we observe a decreasing mobility from samples C and D, which are strongly limited by the interface charges. To fit the observed behavior, we propose that some of the charged defects show a thermal activation, leading to an increase in ionized defects at elevated temperatures. In the calculations, we have used interface charge defects in the form of $n_i = n_i^0 + C\times\exp(-E_a/k_BT)$, where the interface charge defect density at low temperatures n_i^0, the constant C, and activation energy E_a are fitted to experimental data, with the fitted values given in the insets of Fig. 4. We find that the bare semiconductor surfaces have an total ionized defect density of around 2–3 $\times 10^{14}\,\text{cm}^{-2}$, which is reduced by ~3× by the high-k passivation.

In summary, we have investigated the electron transport properties of near surface InGaAs quantum wells by comparing Hall mobility measurements with scattering calculations to estimate the charged impurity density at the surface. In buried quantum wells, the mobility is greatly enhanced due to the reduced effect from charged impurity scattering on the mobility, resulting in mobilities of 7900 and 10 000 cm^2/V s. The passivation of an ALD oxide is beneficial for quantum wells situated directly at the surface, due to a reduced charge impurity density, increasing the mobility from 1500 cm^2/V s to 2600 cm^2/V s.

This work was supported in part by the Swedish Research Council, in part by NanoLund, in part by the Swedish Foundation for Strategic Research, and in part by the European Union H2020 program SEQUENCE (Grant No. 871764).

DATA AVAILABILITY

The data that support the findings of this study are available from the corresponding author upon reasonable request.

REFERENCES

[1] J. Lin, X. Cai, Y. Wu, D. A. Antoniadis, and J. A. del Alamo, IEEE Electron Device Lett. **37**, 381 (2016).
[2] A. Tessmann, A. Leuther, F. Heinz, F. Bernhardt, L. John, H. Massler, L. Czornomaz, and T. Merkle, IEEE J. Solid-State Circuits **54**, 2411 (2019).
[3] L. Casparis, M. R. Connolly, M. Kjaergaard, N. J. Pearson, A. Kringhøj, T. W. Larsen, F. Kuemmeth, T. Wang, C. Thomas, S. Gronin, G. C. Gardner, M. J. Manfra, C. M. Marcus, and K. D. Petersson, Nat. Nanotechnol. **13**, 915 (2018).
[4] J. S. Lee, B. Shojaei, M. Pendharkar, M. Feldman, K. Mukherjee, and C. J. Palmstrøm, Phys. Rev. Mater. **3**, 014603 (2019).
[5] J. Shabani, A. P. McFadden, B. Shojaei, and C. J. Palmstrøm, Appl. Phys. Lett. **105**, 262105 (2014).
[6] K. S. Wickramasinghe, W. Mayer, J. Yuan, T. Nguyen, L. Jiao, V. Manucharyan, and J. Shabani, Appl. Phys. Lett. **113**, 262104 (2018).
[7] S. J. Pauka, J. D. S. Witt, C. N. Allen, B. Harlech-Jones, A. Jouan, G. C. Gardner, S. Gronin, T. Wang, C. Thomas, M. J. Manfra, D. J. Reilly, and M. C. Cassidy, arXiv:190808689 (2019).

© Author(s) 2020

[8]M. I. Abdalla, D. G. Kenneson, and W. Powazinik, in International Conference on Indium Phosphide and Related Materials (1990), p. 108.
[9]P. Ramvall, N. Carlsson, P. Omling, L. Samuelson, W. Seifert, M. Stolze, and Q. Wang, Appl. Phys. Lett. **68**, 1111 (1996).
[10]R. D. Long, B. Shin, S. Monaghan, K. Cherkaoui, J. Cagnon, S. Stemmer, P. C. McIntyre, and P. K. Hurley, J. Electrochem. Soc. **158**, G103 (2011).
[11]M. E. Rudinsky, S. Yu. Karpov, H. Lipsanen, and A. E. Romanov, Mater. Phys. Mech. **24**, 278 (2015); available at http://www.ipme.ru/e-journals/MPM/no_32415/MPM324_10_rudinsky.pdf.
[12]H. Sakaki, T. Noda, K. Hirakawa, M. Tanaka, and T. Matsusue, Appl. Phys. Lett. **51**, 1934 (1987).
[13]B. K. Ridley, J. Phys. C **15**, 5899 (1982).
[14]T. Matsuoka, E. Kobayashi, K. Taniguchi, C. Hamaguchi, and S. Sasa, Jpn. J. Appl. Phys., Part 1 **29**, 2017 (1990).
[15]P. J. Price, Ann. Phys. **133**, 217 (1981).
[16]P. K. Basu and B. R. Nag, J. Phys. C **14**, 1519 (1981).
[17]A. Gold, Phys. Rev. B **35**, 723 (1987).
[18]M. Jonson, J. Phys. C **9**, 3055 (1976).
[19]G. Bastard, Appl. Phys. Lett. **43**, 591 (1983).

© Author(s) 2020